Princeton Plasma Physics Laboratory

PPPL- 4472

PPPL- 4472

Lower Hybrid Heating and Current Drive on the Alcator C-Mod Tokamak

J.R. Wilson, R. Parker, M. Bitter, P.T. Bonoli, C. Fiore, R.W. Harvey, K. Hill, A.E. Hubbard, J.W. Hughes, A. Ince-Cushman, C. Kessel, J.S. Ko, O. Meneghini, C.K. Phillips, M. Porkolab, J. Rice, A.E. Schmidt, S. Scott,S. Shiraiwa, E. Valeo, G.Wallace, J.C. Wright and the Alcator C-Mod Team.

November, 2009

Prepared for the U.S. Department of Energy under Contract DE-AC02-09CH11466.

Princeton Plasma Physics Laboratory
Report Disclaimers

Full Legal Disclaimer

Trademark Disclaimer

PPPL Report Availability

Princeton Plasma Physics Laboratory:

http://www.pppl.gov/techreports.cfm

Office of Scientific and Technical Information (OSTI):

http://www.osti.gov/bridge

Related Links:

U.S. Department of Energy

Office of Scientific and Technical Information

Fusion Links

Lower Hybrid Heating and Current Drive on the Alcator C-Mod Tokamak

J R Wilson[1], R Parker[2], M Bitter[1], P T Bonoli [2], C Fiore[2], R W Harvey[3], K Hill[1], A E Hubbard[2], J W Hughes[2], A Ince-Cushman[2], C Kessel[1], J S Ko [2], O Meneghini[2], C K Phillips[1], M Porkolab[2], J Rice[2], A E Schmidt[2], S Scott[1], S Shiraiwa[2], E[1] Valeo[1], G. Wallace[2], J C Wright[2] and the Alcator C-Mod Team

[1]Princeton Plasma Physics Laboratory, Princeton University, Princeton, NJ 08543, USA
[2]Plasma Science and Fusion Center, MIT, Cambridge, MA 02139, USA
[3]CompX, Po Box 2672, Del Mar, CA 92014-5672, USA

E-mail: jrwilson@pppl.gov

Abstract. On the Alcator C-Mod tokamak, lower hybrid current drive (LHCD) is being used to modify the current profile with the aim of obtaining advanced tokamak (AT) performance in plasmas with parameters similar to those that would be required on ITER. To date, power levels in excess of 1 MW at a frequency of 4.6 GHz have been coupled into a variety of plasmas. Experiments have established that LHCD on C-Mod behaves globally as predicted by theory. Bulk current drive efficiencies, $n_{20}I_{lh}R/P_{lh} \sim 0.25$, inferred from magnetics and MSE are in line with theory. Quantitative comparisons between local measurements, MSE, ECE and hard x-ray bremsstrahlung, and theory/simulation using the GENRAY, TORIC-LH CQL3D and TSC-LSC codes have been performed. These comparisons have demonstrated the off-axis localization of the current drive, its magnitude and location dependence on the launched $n_{||}$ spectrum, and the use of LHCD during the current ramp to save volt-seconds and delay the peaking of the current profile. Broadening of the x-ray emission profile during ICRF heating indicates that the current drive location can be controlled by the electron temperature, as expected. In addition, an alteration in the plasma toroidal rotation profile during LHCD has been observed with a significant rotation in the counter current direction. Notably, the rotation is accompanied by peaking of the density and temperature profiles on a current diffusion time scale inside of the half radius where the LH absorption is taking place.

PACS: 52.50.Sw, 52.55.Wq

1. Introduction

The Alcator C-Mod program has as one of its goals the aim of producing advanced tokamak (AT) discharges. In order to provide the current profile control required for obtaining reduced or reverse shear a lower hybrid (LH) rf power system [1] has been installed on the tokamak. One of the advantages of exploring the applicability of LH current drive on Alcator C-Mod is the equivalence of many of the important parameters, such as plasma density, magnetic field, and rf frequency to those required for a reactor, and in particular ITER. In addition, C-Mod uses heating sources that provide low torque to the plasma, as would be true for a reactor, and the time constants involved allow for relaxation of the relevant profiles. Initial experiments [2,3] have demonstrated that the system behaves as expected with bulk current drive efficiencies $\eta = n_{20}I_{lh}R/P_{lh} \sim 0.25$ in line with theory and expectations from previous experiments. Recent work, reported in this paper, concentrates on detailed measurements of the spatial location of the driven current, the role of fast electron diffusion in spreading the current and other effects of applying LH power to the plasma. In addition, to extrapolate the application of LHCD for use in future devices a program of model development and validation is underway. The plan of this paper is as follows. The local measurements of fast electrons and CD derived from hard x-ray measurements and MSE along with comparisons to modeling will be

described in Section 2. Section 3 includes a brief description of the effect of LHCD on plasma rotation. In Section 4 a discussion of using LHCD in conjunction with ICRF and H-modes will be presented. Application of LHCD in the current ramp phase of the discharge will be discussed in Section 5 and a summary and future plans will be given in Section 6.

2. Local Measurements of Current Drive and Comparison to Modeling

Experiments in which ~400 kW LH power was square-wave modulated with a 25 ms period have been carried out for various densities, launcher phase, and plasma currents. The hard x-rays detected from these experiments contain information about the build-up and slowing-down of the fast electron tail. The x-rays counts are boxcar binned (2.5 ms bins) for high time-resolution measurements. These experiments are also ideal for modeling, because the magnetic geometry does not have time to change during the short 12.5 ms LH pulse. Figure 1 shows inverted time-resolved hard x-ray profiles for 3 different values of the launched $n_{||}$ in low-density discharges, $\bar{n}_e = 8\times10^{19}m^{-3}$. The solid lines correspond to times when the

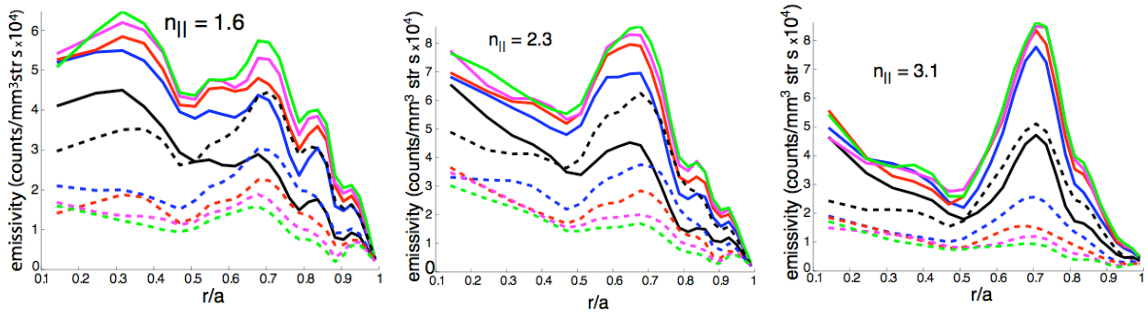

FIG. 1 Time evolution of radial profiles (black, blue red, purple, green) of hard x-ray emissivity (40-60 keV) for three different values (1.6, 2.3 and 3.1) of launched $n_{||}$. With 0.4 MW modulated LH power

LH power is on and the dashed lines correspond to times when the LH power is off. Each line is a bin of 2.5 ms. The fast electron tail build-up comes to steady state before the LH pulse turns off. Inversions were performed using a regularized least-squares fit that assumes x-ray emissivity is a flux function. A clear trend with phase is apparent, with higher launched $n_{||}$ corresponding to greater off-axis localization of fast electrons, in agreement with modeling. For the $n_{||}$ = 1.6 case modeling indicates that the central (r/a ~0.3) peak corresponds to rays that pass near the center while the peak near r/a ~ 0.7 corresponds to rays that miss the central region and upshift in $n_{||}$ before damping. The location of the peak of the x-ray profile can also be varied by changing the target temperature with ICRF heating. Figure 2 shows the peak of the x-ray emission moving further off-axis with the application of ICRF.

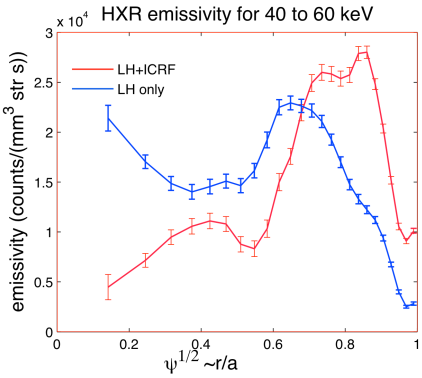

Fig. 2 *radial profile of x-ray emission with and without ICRF heating*

An effort has been made to obtain the EFIT equilibrium reconstruction of LHCD plasmas, which is consistent with an MSE diagnostic [4] and the sawtooth inversion radius. An EFIT equilibrium during the pre-LH phase is used for a reference. This reference equilibrium has a q=1 surface at the sawtooth inversion radius inferred from ECE signals.

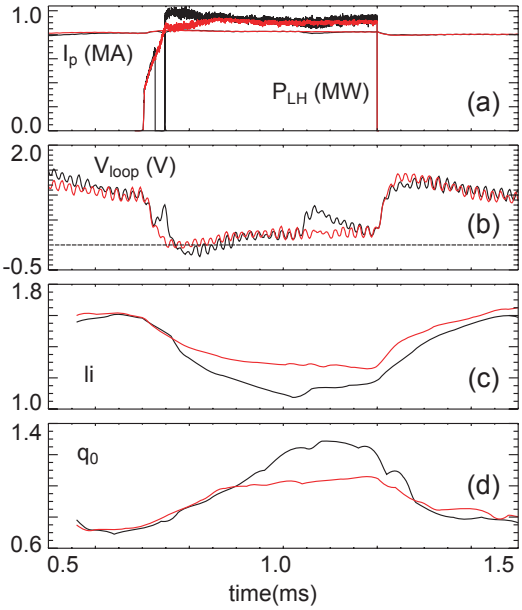

Figure 3. *Time evolution of two LH discharges showing reduction in loop voltage, decrease in plasma inductance and increase in central safety factor.* $n_{||} = 1.5$ *(black),* $n_{||} = 1.9$ *(red)*

Since the MSE system in Alcator C-Mod currently experiences shot-to-shot drift due to thermal stress-induced birefringence [5], only the relative change of pitch angles between the pre-LH phase and the LH phase is used to determine the poloidal magnetic field during LHCD. By constraining the poloidal field in EFIT in this way, consistency of the q profile evolution with the disappearance and re-appearance of the sawtooth activity is realized in the reconstructed LHCD equilibrium. Reasonable agreement with the kinetic stored energy independently calculated using T_e, n_e and Z_{eff} is also obtained. Figure 3 shows two LHCD discharges with different $n_{||}$'s. In both cases, a decrease of internal inductance and increase of central safety factor is observed, indicating off-axis current drive by LHCD. The lower $n_{||}$ case shows larger changes in l_i and q_0, consistent with the increase of current drive efficiency at lower $n_{||}$. Even though the lower value of $n_{||}$ drives current closer to the axis, since we are constraining the discharge to have constant current the higher efficiency of current drive at lower $n_{||}$ dominates over the radial location effect. The mid-plane current density profiles obtained from the MSE+ECE constrained EFIT method are shown by the solid lines in Fig. 4a. A similar approach was used by Naito et al. [6]. The mid-plane current density profile can also be obtained from the MSE pitch angle data directly using an analytic formula derived by Petty et al. [7]. EFIT equilibria in the pre-LH phase together with the MSE data are used to reconstruct the poloidal field during LHCD, as described above, and the mid-plane current density is calculated using the approach in [7]. The results are shown as points in Fig 4a. For better statistics, the average of the poloidal field changes from 4 identical discharges were used to determine j(r) for each $n_{||}$. Although the profiles from both methods successfully show the reduction of the current density near the magnetic axis during LHCD, and the $n_{||}$ dependence in the profile, they differ in the magnitude of the reduction in central current density. This is likely due to poor radial resolution near the magnetic axis where the radial resolution of the MSE is comparable with the spacing of the EFIT flux surfaces. The observation that the difference between the two methods decreases in the next innermost channel in both $n_{||}$ cases supports this postulate. Except for the innermost channels, the

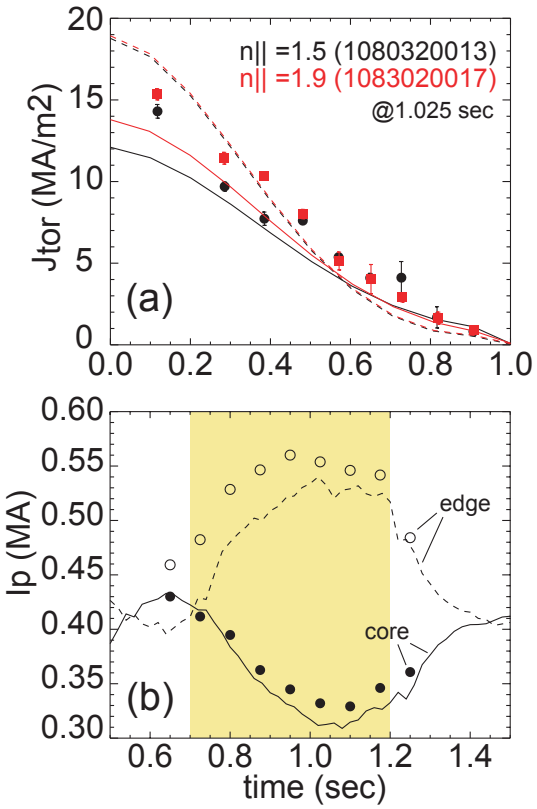

Figure 4. *Effect of LHCD on Current profile (a) Direct current density (points) and analytic formula via MSE for the two discharges in fig.2 and pre-LH phase (dashed line). (b) time evolution of "partial" plasma currents showing reduction in core (r/a < 0.44) current and increase in edge (r/a > 0.44) current during the* $n_{||} = 1.5$ *LH pulse (yellow).*

more direct method also indicates local variations in the profile that the MSE+ECE constrained EFIT approach cannot show, since low-order polynomials are used to model p' and FF'.

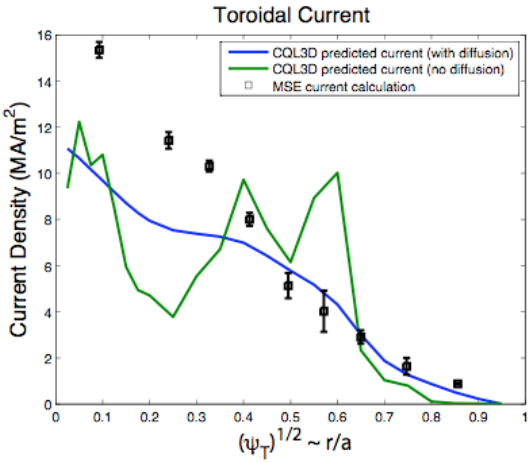

Figure 5. *Toroidal current density profiles derived from MSE measurements and predicted by the GENRAY/CQL3D model (with and without fast electron diffusion)*

Another way to illustrate the off-axis current drive during the LH phase is to compare "partial" plasma currents. Figure 4(b) shows the time evolution of such currents flowing in two regions. The

core current is the total current contained inside r/a = 0.44 and the edge current is that outside that radius. The currents for the direct MSE method are obtained by simply integrating the toroidal current profiles on the mid-plane of the low field side, neglecting the neoclassical Pfirsch-Schluter current. Again, the results from the MSE+ECE constrained EFIT and the direct MSE methods are shown together. Besides the offsets in the absolute values, both methods show clear redistribution of currents from 'core' to 'edge'. Also, note that MHD activity took place at 1.05 s, leading to degradation in the current drive. The time scale of the change of current profile is consistent with an estimated current re-distribution time, 160 ms, using $\tau = 1.4\kappa a^2 T_e^{1.5}/Z_{eff}$, where $\kappa = 1.6$, a = 0.23 m, $T_e = 2.5$keV, and $Z_{eff} = 3.0$ are used, respectively.

Detailed GENRAY/CQL3D modeling has been carried out for this steady-state LH discharge for comparison with the MSE measurements. The modeled results are shown here (Fig. 5), with and without radial diffusion. The modeled case with diffusion uses a spatially uniform diffusion coefficient of .04 m^2/s with a velocity dependence of $(v_{||}/v_{th})/(\gamma^3)$ [8]. The value 0.04 was chosen to make the agreement between r/a =0.5 and 0.7 reasonable. The magnetic equilibrium corresponding to the pre LH phase of the discharge used as input to the code was obtained using an MSE-constrained, sawtooth-inversion-radius-constrained EFIT analysis. The modeling here shows diffusion to be an important effect, smoothing the current profile to more closely resemble that measured by MSE. Both the MSE measured current profile and the profile modeled with diffusion feature a current "bump" in slightly different radial locations.

Most modeling to date has used the GENRAY/CQL3D package that models the wave propagation via a WKB ray-tracing procedure. An electromagnetic field solver TORIC LH, valid in the lower hybrid range of frequencies (LHRF) has been developed and applied to LHRF experiments in Alcator C-Mod [9]. The field solver couples the electrostatic “slow” wave through a waveguide boundary condition on the parallel electric field and also retains the electromagnetic “fast” wave branch. The wave electric field is expressed using a semi-spectral ansatz consisting of a sum over poloidal Fourier modes. Simulations are performed on a massively parallel computing cluster in order to retain the mode resolution needed to resolve the short wavelengths characteristic of the LHRF regime. This simulation capability is currently being used to explore the importance of full-wave effects in the LHRF regime such as focusing, diffraction, and wave front reconstruction at cut-offs. Detailed comparisons are discussed in a companion paper [10]. In general the two methods are found to be in reasonable agreement even in the multi-pass regime with the full wave code also showing some on and off-axis absorption. In both cases including fast electron diffusion spreds and smooths the absorption more in line with the results of fig. 1. If too much diffusion is included the current drive efficiency is too low and fig. 3 cannot be reproduced. Experiments in Alcator C-Mod are mostly in the multi-pass regime for present parameters ($T_e < 5$keV). The full-wave solver has also now being coupled to the bounce averaged electron Fokker Planck code CQL3D [11]. This will allow detailed comparisons to be made between experimentally measured profiles of hard x-ray emission and a synthetic diagnostic code in CQL3D employing the fully converged non-thermal electron distribution function, obtained by iterating the full-wave and Fokker Planck solvers.

3. Toroidal plasma rotation change induced by LHCD

The application of LHCD in C-Mod is typically accompanied by a change in the toroidal rotation of the plasma [12]. The rotation is seen to increment in the counter current direction in the plasma core. The magnitude of the change is correlated with the drop in internal inductance, l_i, and scales with LH power and plasma density as if it is directly proportional to the LH driven current. Figure 6 shows the time evolution of a 0.8 MA L-mode plasma with 0.8 MW of lower hybrid power with a launched $n_{||}$ of 2.3. Modeling indicates ~250 kA of LHCD for this discharge. The rotation change occurs over the inner half radius. The time scale for the change is consistent with the current relaxation time and much longer than the energy or momentum confinement times. If the lower hybrid power is applied with an $n_{||}$ that only results in plasma heating no change in rotation is observed. Figure 7 shows the proportionality between the magnitude of the rotation change and the magnitude of the change of inductance for a variety of launched $n_{||}$’s. Note that the magnitude is largest for the fastest waves even

though the wave momentum input from the LHCD is proportional to $n_{||}$. This would indicate that the wave

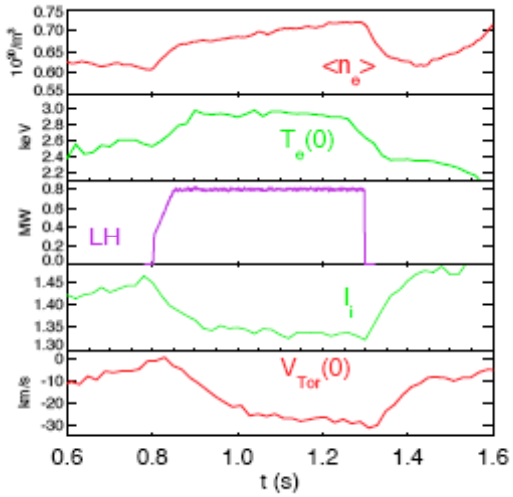

Figure 6. *Change in $\bar{n}_e$, T_{e0}, l_i , and central plasma rotation during LHCD.*

momentum is not the direct source of the torque on the plasma. Figure 8 shows radial structure of the affected profiles. The rotation change peaks on axis and exists inside of the radius where the current drive is expected to be occurring from modeling. The density and temperature profiles also peak modestly inside this radius.

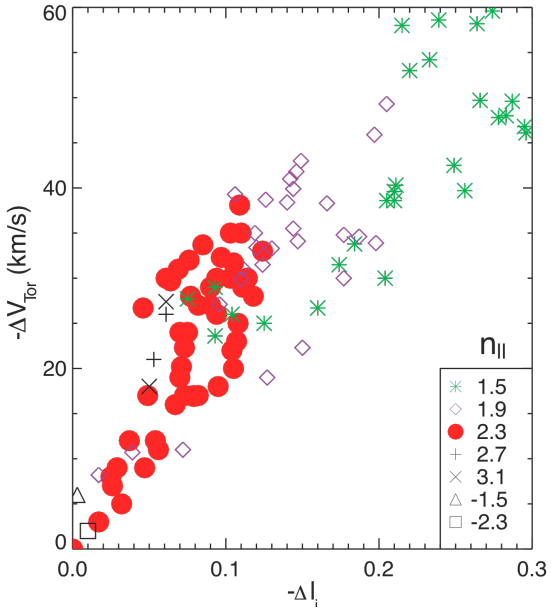

Figure 7. *Change in toroidal velocity versus change in internal inductance for various $n_{||}$*

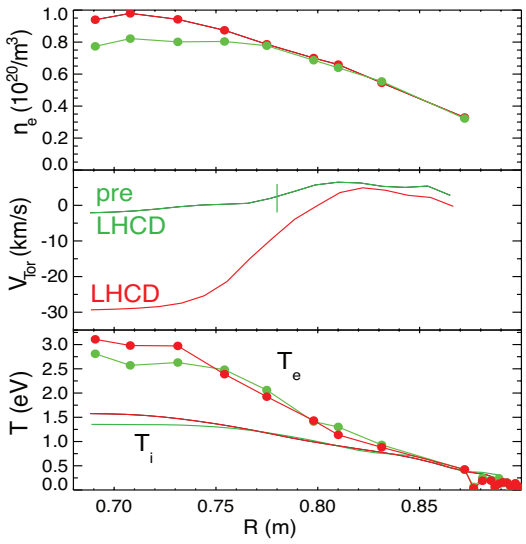

Figure 8. *Plasma profile of density, toroidal rotation and temperature before and after LH induced rotation change*

4. LHCD effects in H-modes and H-mode target plasmas

The advanced scenarios that are the primary motivation for the implementation of LHCD on C-Mod require active modification of the current profile in discharges with significant bootstrap fraction. This requires combining LHCD with high ICRF power, in high confinement discharges with core and/or edge transport barriers. H-mode discharges on C-Mod are particularly challenging for LHCD due to high pedestal densities and short (few mm) scale lengths, raising concerns about coupling and deposition in regions of steep density gradients. In addition operation in conjunction with high power ICRF has proven to require local edge density enhancement by gas puffing on both JET and Tore Supra. [13] On C-Mod, reductions in the density immediately in front of the LH launcher have been observed when ICRF power is applied to an antenna having a short magnetic connection link to the LH launcher. A simple system consisting of two gas injection capillary tubes was installed on the C-Mod LHCD antenna. This gas injection system provided a local increase in the electron density immediately in front of the LH antenna without raising the core density and thereby decreasing the current drive efficiency. The two independently controlled capillaries are located in the upper right

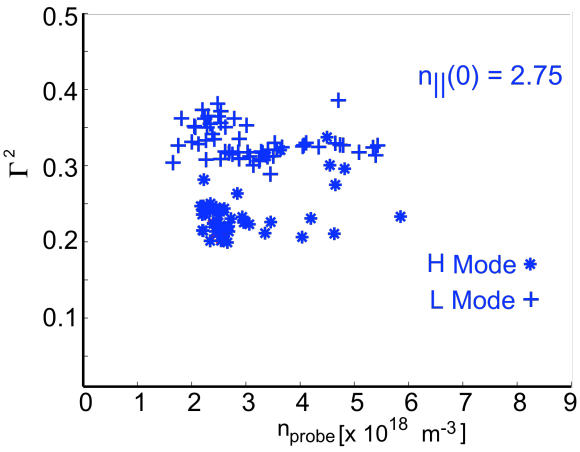

Figure 9. *Power Reflection coefficient versus density measured by Langmuir probe at the LH launcher.*

and lower left corners of the "box" formed by the guard limiters. Initial tests of the capillaries with no LH power showed a localized source of visible light emission centered around the capillary locations. Subsequent tests at a range of power levels indicate a strong increase in the local electron density in front of the LH antenna during high power operation. In general, this puffing has not proved necessary for successful operation in H-mode plasmas. LH coupling into H-mode plasmas, as determined by average reflection coefficients, is comparable to or even better than L-modes (Fig. 9), although fluctuations in Γ can be higher. Pedestal densities have been minimized through dynamic variation of the magnetic topology, sweeping from lower null (favorable drift) to upper null [14], by using a new in-vessel cryopump [15] and by increasing q_{95}. Steady EDA H-modes with $\bar{n}_e$ = 1.7-2×10^{20}m^{-3} and n_{ped} = 1.2-1.7×10^{20}m^{-3} have been achieved. While much higher than is typical of LHCD experiments elsewhere, these densities are lower than typical C-Mod H-modes and, at B_T=5.4 T, are accessible to LH waves with $n_{||} > 2$. An interesting and unexpected effect of applying LHCD in such H-modes is illustrated in Fig. 10. In many cases the pedestal and core density, and also radiated power, decreased during the LH phase, indicating an increase of particle transport. Pedestal temperature increased, by up to 50%, leading to a significant decrease in edge collisionality (Fig. 11). Central T_e also increases consistent with stiff profiles [16]. Stored energy increased during LHCD, and confinement times remained constant, indicating that LH power is absorbed in the confined plasma. This mechanism for this density "pump-out" effect is not yet understood. It has been observed in clean H-mode discharges with I_p=450-600 kA and increases with LH input power. Density reduction has been seen in cases with $n_{||}$ varied from 1.9, for which waves were marginally accessible to the edge, to 2.8, for which reduced current drive efficiency is expected. This suggests that a direct wave effect, rather than the modification of j(r), might be responsible. High radiated power and/or impurity level diminishes or eliminates the density reduction.

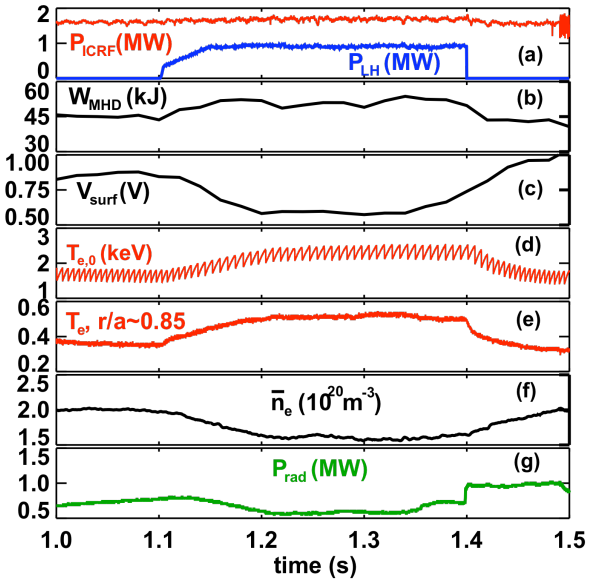

Figure 10. *Time evolution of C-Mod H-mode discharge (610 kA, 5.4 T), with addition of 0.9 MW LHCD from 1.1 to 1.4 s (a). Notable changes include a decrease in electron density (f) and radiated power (g), and accompanying increase of edge Te (e) as well as core Te. (d) Stored energy (b) increases, while surface loop voltage (c) decreases significantly.*

The density pump-out effect has not been observed in L-mode discharges, suggesting a connection to pedestal transport, possibly useful for control purposes. Given the strong increase in T_e during the LHCD phase, determining the degree of current drive in these H-mode plasmas is not straightforward despite significant decreases in V_{loop} and l_i.

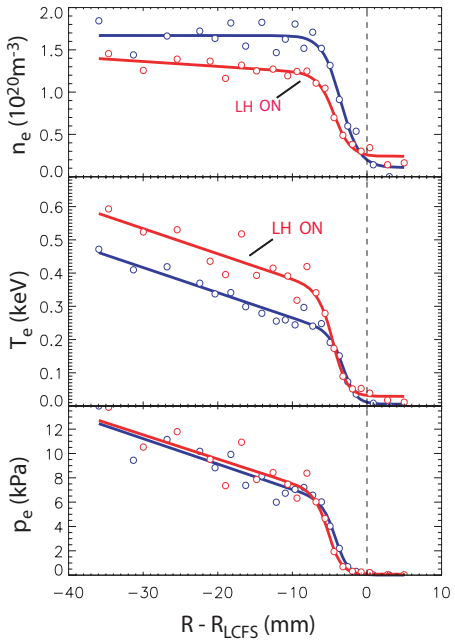

Figure 11. *Pedestal density, temperature, and pressure before and after application of LHCD*

Modeling of the discharge shown in fig. 9, using the TRANSP code with LSC [17], predicts 30-40 kA of LHCD, localized off axis with a peak at r/a=0.65. Extrapolation to the planned upgrade power of 2.7 MW predicts ~150 kA in comparable discharges, in line with advanced scenario modeling [18]. Further reduction of density would clearly be desirable.

5. Use of LHCD during the current ramp

LHCD is being applied in the current ramp-up and flattop phase. The plasma current is ramped up in 500 ms to either 450 or 600 kA. The effectiveness of the LH modification of the current profile is measured by the delay in the onset of the sawtooth instability, clearly visible on the Grating Polychromator (GPC) temperature mesurement.

Shown in Fig. 12 is the central ECE signal versus time over the first 800 ms, for four discharges. While ECE in some cases has non-thermal contributions, it clearly shows the onset of the sawtooth instability, noted by the vertical dashed lines. Sawteeth begin in the ohmic case at 170 ms. The addition of 0.5 MW of LH with $n_{||}$ =2.3 delays the sawteeth by about 540 ms. When the same level of LH power is combined with 1 MW of ICRF heating (80 MHz, minority H) the onset is delayed by 450 ms, and with 2 MW of ICRF it is delayed by 280 ms. The reduced delay with increasing ICRF power is consistent with the behavior of the delay as a function of density (see below). The plasma remains in L-mode over the times of interest.

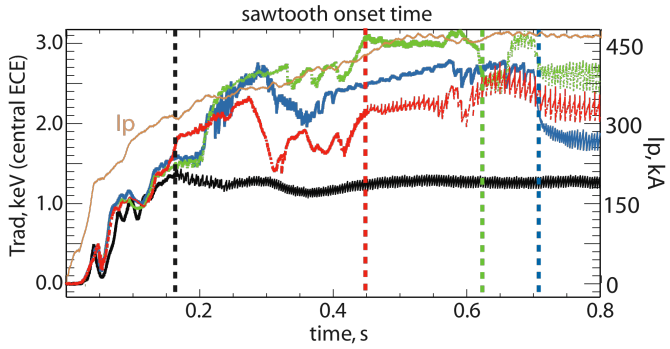

Figure 12. *Time evolution of central ECE for four discharges – Ohmic (black), 0.5 MW LH (blue), 0.5 MW LH +1 MW ICRF (green) and 0.5 MW + 2 MW ICRF (red).*

Shown in Fig. 13 is the variation of the sawtooth onset with the plasma density, the lowest density, $\bar{n}_e = 4\times10^{19}m^{-3}$, delaying the sawtooth by 540 ms, the intermediate density, $\bar{n}_e = 7\times10^{19}m^{-3}$, delaying it by 295 ms, and the highest density, $\bar{n}_e = 9\times10^{19}m^{-3}$, by only 130 ms.

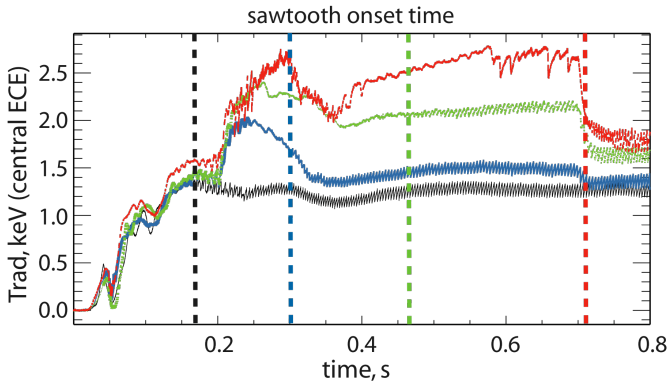

Figure 13. *Time evolution of central ECE for 0.5 MW of LH applied to plasmas with $\bar{n}_e=4x10^{19}m^{-3}$ (red) $\bar{n}_e=7x10^{19}m^{-3}$ (green) and $\bar{n}_e=9x10^{19}m^{-3}$ (blue) densities. Ohmic comparison in black with $\bar{n}_e=9x10^{19}m^{-3}$.*

In Fig. 14 the internal self-inductance $l_i(1)$ is shown during this discharge phase, confirming that the current profile has been broadened the most in the low density and higher LH driven current case. Overall the introduction of LH power into the ramp-up phases of lower plasma current (450-600 kA) discharges has demonstrated strong current profile modification through modification of the onset of

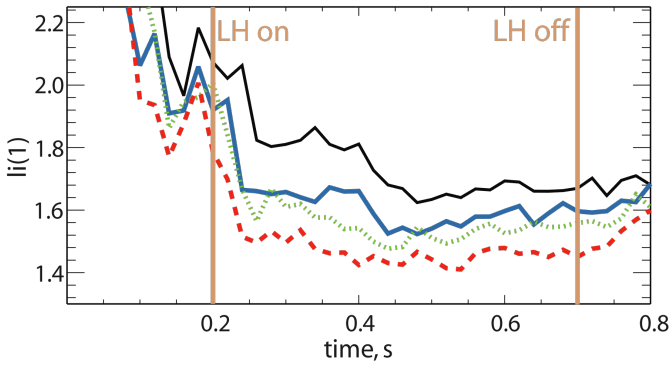

Figure 14. *Time evolution of internal inductance for the same discharges as in fig. 12.*

the sawtooth instability. Analysis of the 600 kA discharge with 0.4 MW of LH power using TSC/LSC code [17], indicates that a large LH current of about 220 kA is driven initially during the ramp, assisted by the background electric field. This current persists at this level through the ramp, and then relaxes to about 65 kA in the flattop phase. The simulation shows that the introduction of the LH causes an abrupt increase in q_0 delaying the sawtooth, which then relaxes allowing the sawtooth instability to emerge. The sawtooth onset time from the simulation was 450 ms versus 350 ms in the experiment. The experiments also show that the delay in the onset of sawteeth is typically less when sufficiently high ICRF power is added to the LH power. Although, at low plasma currents in the ramp-up, the ICRF power typically leads to higher electron temperature earlier, it also generates impurities that lead to higher radiated power and higher Z_{eff}. Simulation of these discharges continues in an effort to understand the evolution more clearly. In other related experiments [18] delay of $q_0 = 1$ onset has been demonstrated at I_p = 0.8 MA (q_{95}=4.2), in the range required for hybrid scenario experiments that will help assess the properties of this regime on ITER.

6. Summary and Future work

Lower hybrid heating and current drive experiments on the Alcator C-Mod tokamak have been extended to detailed measurements of the driven current and comparisons to models as well as application of LHCD to plasma scenarios that will lead to eventual advance tokamak conditions for several current relaxation times. Measurements of the time and space resolved hard x-ray profiles have been compared to modeling with the GENRAY/CQL3D code. A new full wave code TORIC-LH is under development and will also be coupled to CQL3D. Direct measurements of the driven current with the MSE diagnostic have been compared to the code and support the conclusion that a small ~0.04 m^2/s rate of fast electron diffusion is taking place. The LH driven current is observed to take place off-axis and its location and magnitude is sensitive to the launched $n_{\|}$. Changes in the toroidal rotation velocity in the counter current direction are observed with the magnitude of the change proportional to the inferred driven current. In order to obtain advanced scenarios in Alcator C-Mod, LHCD must be applied in conjunction with high power ICRF and in H-mode plasmas. Successful coupling to H-mode plasmas has been obtained with low power reflection coefficients, in spite of the short density scrape off lengths. Operation with simultaneous high power ICRF has only proven difficult for antennas that are connected to the lower hybrid launcher with short magnetic connection lengths. Reductions in the edge collisionality are observed in H-mode discharges with a drop in the edge density accompanied with an increase in the edge temperature such that the edge pressure is equal or slightly increased. The increased edge temperature is then reflected throughout the discharge leading to an increase in confinement. Modeling with TRANSP of these discharges indicates that they should extrapolate to an attractive AT plasma for 2.7 MW of injected LH power. Such levels are envisioned for the completed LH system with the addition of a second launcher and increase in the available klystron power to 4 MW. Experiments utilizing LHCD during the current ramp-up phase of the discharge also demonstrate the feasibility of using LHCD to broaden the current profile as demonstrated by the delay in the onset of the sawtooth instability by as much as 0.5s. In the immediate future a new lower hybrid launcher will be installed on C-Mod allowing a higher fraction of the rf power to be coupled into the discharge. Presently, slightly greater than 50% of the source power is lost between the klystron output and the plasma due to losses in the transmission line, power splitting network and grill, all of which should be reduced in the new design. This upgrade will allow for experiments at higher injected power to be carried out in the near future.

Acknowledgements

This work performed under USDOE Contract numbers DE-FC02-99ER54512 and DE-AC02-76CH03073.

References

[1] Bonoli P T *et al.* 2007 *Fusion Science and Technology* **51** 401-436
[2] Wilson J R, Bernabei S, Bonoli P, Hubbard A, Parker R, Schmidt A, Wallace G and Wright J 2007 *Proceedings of the 17th Topical Conference on RF Power in Plasmas*, **933** (AIP) Clearwater, Florida 269-276
[3] Bonoli P T *et al.,* 2008 *Physics of Plasmas* **15** 056117
[4] Basse N P *et al.,* 2007 *Fusion Science and Technology* **51**, 476-507
[5] Ko J, Scott S, Bitter M and Lerner S 2008 *Reviews of Scientific Instruments* **79**(10) 10F520
[6] Naito O, *et al.* 2002 *Physical Review Letters* **89** 065001-1-4
[7] Petty C C, Politzer P and Lin-Liu Y R 2005 *Plasma Physics And Controlled Fusion* **47** 1077-1100
[8] Texter S, Porkolab M, Bonoli P, Knowlton S and Takase Y 1993 *Physics Letters A* **175** 428-432
[9] Wright J C, Valeo E, Phillips C K, Bonoli P T and Brambilla M 2008 *Communications in Computational Physics,* **4** 545-555.
[10] Wright J C *et al*, 2009 *Proceedings of the* 22nd *Conference on Fusion Energy*, (IAEA) paper TH/P3-17

[11] Harvey, R.W. and McCoy, M.G. 1993 *Proceedings of the IAEA Technical Meeting on Numerical Modeling of Plasmas* (Montreal, Canada, 1992) (Vienna: IAEA).
[12] Rice J. *et al.* 2008 *Proceedings of the* 22nd *Conf. on Fusion Energy,* (IAEA) paper EX/P5-4.
[13] Rantamaki K *et al.* 2007 *Proceedings of the 17th Topical Conferemce on RF Power in Plasmas,* **933** Clearwater, Florida (2007) 261-264
[14] Hughes J W *et al.* 2008 *35th EPS Conference on Plasmas Physics* **32** P1.005
[15] Marmar E A *et al.* 2008 *Proceedings of the 22nd Conference on Fusion Energy* (IAEA) paper OV/4-4
[16] Greenwald M *et al*. 1997 *Nuclear Fusion* **37** (6) 793-808
[17] Ignat D W, Valeo E. and Jardin S C 1994 *Nuclear Fusion* **34** (6) 837-852
[18] Bonoli P, Porkolab M, Ramos J J, Nevins W and Kessel C 1997 *Plasma Physics and Controlled Fusion* **39** 223-236
[19] Sips G *et al.* 2008 *Proceedings of the 22nd Conference on Fusion Energy* (IAEA) paper IT/2-2

The Princeton Plasma Physics Laboratory is operated
by Princeton University under contract
with the U.S. Department of Energy.

Information Services
Princeton Plasma Physics Laboratory
P.O. Box 451
Princeton, NJ 08543

Phone: 609-243-2245
Fax: 609-243-2751
e-mail: pppl_info@pppl.gov
Internet Address: http://www.pppl.gov